Dalton Transactions

RSC Publishing

PAPER

View Article Online
View Journal | View Issue

Surface modified Eu:$GdVO_4$ nanocrystals for optical and MRI imaging†

Cite this: *Dalton Trans.*, 2013, **42**, 10725

Nuria O. Nuñez,*[a] Sara Rivera,[b] David Alcantara,[b] Jesus M. de la Fuente,[b] Jorge García-Sevillano[c] and Manuel Ocaña[a]

Received 4th February 2013,
Accepted 21st May 2013

DOI: 10.1039/c3dt50676b

www.rsc.org/dalton

A facile solvothermal route has been developed for the preparation of europium doped gadolinium orthovanadate nanoparticles (~70 nm) with tetragonal structure, based on a homogenous precipitation reaction at 120 °C from rare earth precursors (yttrium nitrate and europium nitrate) and sodium orthovanadate solutions using an ethylene glycol–water mixture as the solvent. The effects of the doping level on the luminescence properties were evaluated in order to find the optimum nanophosphors. These nanocrystals were successfully functionalized with amino (two step process) and carboxylate (one-pot process) groups provided by amino-dextran polymers (AMD) and polyacrylic acid (PAA), respectively. It was found that while the luminescent properties of both kinds of functionalized systems were similar, the colloidal stability of the PAA-modified sample was higher, because of which, it was selected to study their cytotoxicity and magnetic properties (relaxivity and phantom analyses) to assess their potentiality as multifunctional probes for both "*in vitro*" optical biolabels and negative contrast agents for magnetic resonance imaging.

1. Introduction

Nowadays, much attention has been paid in the biomedical field to the development of multifunctional nanoparticles suitable for both, optical and magnetic resonance (MRI) imaging applications[1] because they combine the high sensitivity of optical imaging for *in vitro* applications with the excellent spatial resolution and depth for *in vivo* application associated with the MRI imaging.[1c,d,g,h] A large variety of compositions have been proposed. For example, the optical functionality may be afforded by quantum dots,[1b] fluorescent dyes,[1b,2] or rare earth based compounds,[1c–j,3] the latter being preferred due to their lower toxicity and higher photostability.[4] For the MRI functionality, the most frequently used contrast agent is superparamagnetic iron oxide,[1b,g,2–5] although different kinds of nanoparticles containing Gd(III) ions have been also proposed[1f,h,j,6] taking advantage of the magnetic moment and nanosecond time scale electronic relaxation time of the Gd cations.[7] These Gd containing materials may consist of a Gd(III) complex,[8] a diamagnetic matrix doped with Gd cations[1c] or Gd compounds such as $GdPO_4$,[9] Gd_2O_3,[1a,d,j,6] GdF_3,[7] $NaGdF_4$,[1d,f,h,i] to mention a few. Important benefits of using nanoparticles of these Gd compounds instead of Gd(III) complexes are a dramatic increase in the local Gd ion concentration in the region of interest, easy functionalization, control of targeting and release through their particle size, possibility of improvement in relaxivities[1h] and easy doping with other luminescent lanthanide (Ln) cations to obtain the optical functionality.

Among the different luminescent Gd compounds, those based on Gd orthovanadate ($GdVO_4$) are of special interest from the optical point of view since the excitation of the doping Ln cation through an energy transfer from the vanadate anion is much more efficient than the direct excitation of the Ln electronic levels, which results in a higher luminescence.[10] It is outstanding that although several reports have been published on the synthesis and optical properties of Ln:$GdVO_4$ nanoparticles having different morphologies (rods,[11] spindles,[12] and spheres)[13,14] little attention has been devoted to the assessment of their potentiality as multifunctional materials for optical and MRI imaging. In fact, to the best of our knowledge, only a few recently published works[10c,13b,14,15] report on the optical imaging ability, the magnetic relaxivity properties and the cytotoxicity of Ln:$GdVO_4$ (Ln = Eu,[10c] Er/Ho/Tm + Yb[13b,14] or Dy[15] nanocrystals).

It is also well known that for most biotechnological applications, the modification of the nanoparticles surface with

[a]*Instituto de Ciencia de Materiales de Sevilla, CSIC-US, Americo Vespucio 49, 41092, Isla de la Cartuja, Sevilla, Spain. E-mail: nurianu@icmse.csic.es*
[b]*Instituto de Nanociencia de Aragon, Universidad de Zaragoza, Campus Rio Ebro, Edif I+D, C/Mariano Esquillor s/n, 50018 Zaragoza, Spain*
[c]*Dpto. Física de Materiales, C-04. Universidad Autónoma de Madrid, 28049 Madrid, Spain*

†Electronic supplementary information (ESI) available. See DOI: 10.1039/c3dt50676b

molecules of biological interest is an important issue since they provide anchors for adding functional ligands such as antibodies and drugs[16] and affect the colloidal stability of nanoparticles suspensions as recently demonstrated for YVO_4:Eu nanoparticles,[17] which are isostructural to those herein studied. However, among the above-mentioned reports dealing with Ln:$GdVO_4$ nanoparticles, only that by Kang *et al*. was conducted using poly(acrylic) acid functionalized $GdVO_4$ spheres, which were above the nanometric size range (180 nm) and showed a rather irregular shape and a certain degree of aggregation. Moreover, the colloidal stability of an aqueous suspension of such spheres was not addressed by these authors. Therefore, the development of functionalization procedures for $GdVO_4$ based nanophosphors is still highly desirable.

In this work, we have developed simple methods for the synthesis of uniform Eu-doped $GdVO_4$ nanocrystals (70 nm) with optimised luminescent properties, and their functionalization with amino (two step procedure) and carboxylate (one-pot procedure) groups provided by amino-dextran polymers (AMD) and polyacrylic acid (PAA), respectively, in order to comparatively evaluate their colloidal stability in aqueous media (pH = 6.95). In addition, the magnetic relaxivity of the optimum functionalized nanophosphor was analysed through phantom analysis and its cell viability evaluated to assess its potentiality as a biolabel for *in vitro* applications and as MRI contrast agents.

2. Experimental details

2.1. Materials

Gadolinium(III) nitrate hexahydrate ($GdNO_3{\cdot}6H_2O$, Aldrich, 99.9%) and europium(III) nitrate pentahydrate ($Eu(NO_3)_3{\cdot}5H_2O$, Aldrich, 99.9%) were selected as Ln precursors. Sodium orthovanadate (Na_3VO_4, Aldrich, 99.9%) was used as a vanadium source and a mixture of ethylene glycol (EG)–water as a solvent. For functionalization, polyacrylic acid (PAA, average $M_w \sim 1800$, Aldrich) and amino-dextran synthesized polymers were used.

For the amino-dextran (AMD) preparation,[18] aldehyde-dextran was first obtained by oxidation of 1.67 g of dextran (average mol wt 15 000–30 000, Aldrich) dissolved in water (50 cm^3) with 0.8 g of sodium periodate ($NaIO_4$, ≥99.0%, Aldrich). The oxidation was performed overnight at room temperature under magnetic stirring. Once the reaction was finished, the solution was dialyzed against double distilled water for 24 h using a dialysis tubing cellulose membrane. The dextran obtained under these conditions has 20% of the glucose molecules present in the polymer oxidized as di-aldehydes. The aldehyde-dextran so obtained was mixed first with an equal volume of a 3 mol dm^{-3} tetraethylenepentamine (TEPA, ≥98%, Sigma-Aldrich) solution at pH 7.5 (adjusted with NaOH) and then with solid trimethylaminoborane (TMAB, ≥95%, Fluka) which was dissolved until its final concentration reached 150 mM. After 15 h, the obtained amino-dextran was reduced to stabilize the Schiff's bases formed and any remaining aldehyde. For this purpose, 10 mg cm^{-3} of sodium borohydride ($NaBH_4$, ≥98.0% Aldrich) were first added to the above solution after which the pH was adjusted to 10 by adding NaOH. Then, sodium borohydride was added again in a similar proportion (10 mg cm^{-3}). This mixture was kept under magnetic stirring for 2 h at room temperature after which the pH of the mixture was lowered to 6 using hydrochloric acid (37%, Prolabo) to destroy the sodium borohydride excess. Once the dextran was modified with TEPA and reduced, it was dialyzed, first, against a sodium acetate (>99.5%, Fluka) 10 mM solution at pH = 4 and then against double distilled water (twice).

2.2. Nanoparticles synthesis

RE orthovanadate nanoparticles having different Eu/Eu + Gd atomic ratios (0.02, 0.05, 0.10, 0.15) were prepared according to the following procedure. Suitable amounts of RE precursors were dissolved in ethylene glycol (2.5 cm^3). In a separate vial, a weighed amount of Na_3VO_4 was dissolved in an EG–H_2O mixture (1.5 cm^3 H_2O + 1 cm^3 EG). To facilitate the dissolution of reagents in EG the solutions were mildly heated (~80 °C) under magnetic stirring. After cooling down to room temperature, both solutions were then admixed while keeping the magnetic stirring. In the final solutions, the total RE and the Na_3VO_4 concentrations were kept constant at 0.02 mol dm^{-3} and 0.1 mol dm^{-3}, respectively whereas the final EG–H_2O volumetric ratio was 3.5 : 1.5. The so prepared solutions were then aged for 3 h in tightly closed test tubes using an oven preheated at 120 °C. After aging, the resulting dispersions were cooled down to room temperature, centrifuged to remove the supernatants and washed twice with ethanol and once with distilled water. Finally, the precipitates were redispersed in milliQ water or, for some analyses, dried at room temperature.

2.3. Functionalization with amino-dextran

For functionalization, solutions with adjusted pH (8–8.5) of amino-dextran 20% oxidized (0.093 mmol dm^{-3}) were first prepared. Then, a weighed amount of the $Eu_{0.10}Gd_{0.90}VO_4$ nanoparticles previously synthesized was added to such solutions so that their final concentration was 0.2 mg cm^{-3}. The resulting dispersions were sonicated in cold water during 1 h. After this treatment, the so functionalized nanoparticles were washed several times with milliQ water by centrifugation and finally redispersed in milliQ water.

2.4. Functionalization with polyacrylic acid

The Eu-doped $GdVO_4$ nanoparticles functionalized with PAA were obtained following a protocol similar to that described before for the synthesis of Eu-doped $GdVO_4$ particles, which was slightly modified by admixing 2 mg cm^{-3} of PAA into the Na_3VO_4 starting solution.

2.5. Characterization

The shape of the nanoparticles was examined by transmission electron microscopy (TEM, Philips 200CM). For this, a droplet of an aqueous suspension of the samples was deposited on a

copper grid coated with a transparent polymer and dried. The particle size distributions were obtained from dynamic light scattering (DLS, Zetasizer Nano ZS90, Malvern). The crystalline structure of the prepared nanoparticles was identified by X-ray diffraction (Siemens D501). The crystallite size was estimated from the most intense XRD peak of the $GdVO_4$ structure (2 0 0) by using the Scherrer method.

The infrared spectra (FTIR) of the nanophosphors diluted in KBr pellets were recorded in a Jasco FT/IR-6200 Fourier transform spectrometer. Thermogravimetric analysis (TGA) was performed in air at a heating rate of 10 °C min^{-1}, using a Q600TA Instrument. *Z* Potential measurements were carried out in a Malvern Zetasizer Nano-ZS90 apparatus.

For a proper comparison of the luminescent properties of these nanophosphors containing different Eu doping levels, all samples were dispersed in water at the same concentration (0.2 mg cm^{-3}) so that the absorbance of these dispersions in the UV-visible region was similar. The excitation and emission spectra of these samples were measured in a Horiba JobinYvon spectrofluorimeter (Fluorolog FL3-11) operating with a slit of 1.5 nm. Lifetime measurements were obtained under pulsed excitation at 532 nm by using the second harmonic of a Nd:YAG laser (Spectra Physics model DCR 2/2A 3378) with a pulse width of 10 ns and a repetition rate of 10 Hz. The fluorescence was analysed through an ARC monochromator model SpectraPro 500-i and then detected synchronously with an EMI-9558QB photomultiplier and recorded by a Tektronix TDS420 digital oscilloscope. The photographs showing the luminescence of the nanophosphors in water dispersions were taken under illumination with ultraviolet radiation (λ = 312 nm), filtered from a Hg discharge lamp.

^{1}H NMR relaxation times T_1 and T_2 were measured at 1.5 Tesla in a Relaxiometer (Bruker Minispec spectrometer) at different concentrations of nanoparticles (0.1, 0.05, 0.025, 0.0125, 0.00625 mg cm^{-3}) in water at 298 K. T_1 and T_2 values were determined by the inversion-recovery method and by the Carr–Purcell–Maiboom–Gill sequence, respectively. Images were post-processed using dedicated IDL 6.2 (Exelis VIS Inc., Boulder, CA) software with homemade written scripts. Relaxivities (r_1, r_2) were obtained from the slopes of the curves $1/T_{1\ or\ 2}$ *vs.* the concentration of Gd(III) expressed in mM. Phantoms were obtained at 9.4 Tesla in a BrukerBiospec MRI.

The colloidal stability of nanoparticles suspensions (nanoparticle concentration = 0.5 mg cm^{-3}) in milliQ water or in 50 mM MES solutions (2-(*N*-morpholino) ethanesulfonic acid, Sigma, 99%) at pH 6.5 and in completed cell culture was monitored by analyzing the evolution with aging time of their UV-visible absorbance spectrum (UV/VIS Lambda 12 Perkin Elmer spectrometer) and their hydrodynamic diameter obtained from DLS measurements.

2.6. Cytotoxicity assay

Vero cell cultures (monkey kidney epithelial cells) were cultured in Dulbecco's Modified Eagle's Medium (DMEM), supplemented with 10% fetal bovine serum (FBS), 5% glutamine (200 mM) and 5% penicillin (5000 units per mL)/streptomycin (5 mg mL^{-1}). Cell cultures were incubated at 37 °C and equilibrated in 4% CO_2 and air. Cell viability and proliferation were analyzed by the MTT colorimetric assay. For the cytotoxicity assay 5000 cells were seeded in each well of 96-well plates and grown for 24 h. After that, the medium was replaced with fresh medium containing the different types of nanoparticles in varying concentrations. After cultivation again for 24 h or 120 h (in the case of 120 h, the medium was supplemented with FBS (20 μL per well) after 72 h of incubation), 20 μL of MTT dye solution (5 mg cm^{-3} in PBS) was added to each well. After 4 h of incubation at 37 °C and 5% CO_2, the medium was removed, the cells were washed with fresh medium, and formazan crystals were dissolved in 100 μL of DMSO. The absorbance of each well was read on a microplate reader (Biotek ELX800) at 570 nm. The spectrophotometer was calibrated to zero absorbance using culture medium without cells. The relative cell viability (%) related to control wells containing cell culture medium without nanoparticles was calculated by [*A*]test/[*A*]control × 100. Each measurement was repeated at least five times to obtain the mean values and the standard deviation.

3. Results and discussion

3.1. Eu:$GdVO_4$ nanocrystals

Several Eu-doped $GdVO_4$ samples having different Eu content (Eu/Eu + Gd mol ratio = 2, 5, 10, 15%) were synthesized in order to optimize the luminescent properties of these nanophosphors. Irrespective of the Eu content, all samples showed similar morphological (Fig. S1†) and structural characteristics (Fig. S2†), which are illustrated here for the case of $Eu_{0.10}Gd_{0.90}VO_4$ chosen as a representative example. This sample consisted of almost equiaxial nanocrystals (Fig. 1, top), which, according to XRD (Fig. 2), crystallized into the tetragonal $GdVO_4$ structure (ICDD file no. 01-086-0996). The crystallite size value estimated from this XRD pattern was similar (54 nm) to the hydrodynamic diameter (70 nm) (Table 1) obtained from DLS measurements (Fig. S3†), indicating that the nanocrystals presented monocrystalline character and that they do not aggregate in aqueous dispersion.

FTIR spectroscopy was used to gain additional information on samples composition. Thus, the spectrum of the $Eu_{0.10}Gd_{0.90}VO_4$ nanoparticles (Fig. 3) displayed the absorptions associated with vanadate anions (<1000 cm^{-1}),[19] along with broad bands at about 3400 and 1650 cm^{-1} due to adsorbed water, and some much weaker features in the 1500–1300 cm^{-1} region, which can be attributed to the presence of carbonate anions coming from the adsorption of atmospheric CO_2.[10b] TGA analyses (Fig. 4) revealed a total weight loss of ~6 wt% in the 30 °C to 700 °C temperature range due to the release of such impurities (~4 wt% of surface-adsorbed water between 25 and 230 °C and ~2 wt% of carbonate anions at >250 °C). Since no additional absorptions could be observed in the FTIR spectrum of the sample, the presence of EG species on the nanoparticles surface, previously observed for

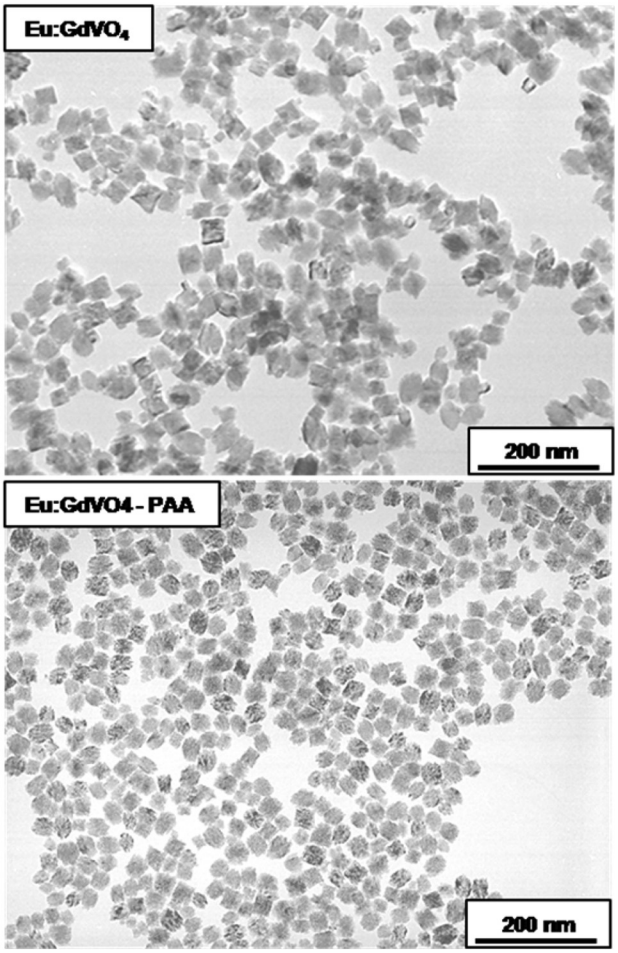

Fig. 1 TEM micrographs of the $Eu_{0.10}Gd_{0.90}VO_4$ nanocrystals unfunctionalized (top) and functionalized with PAA (bottom).

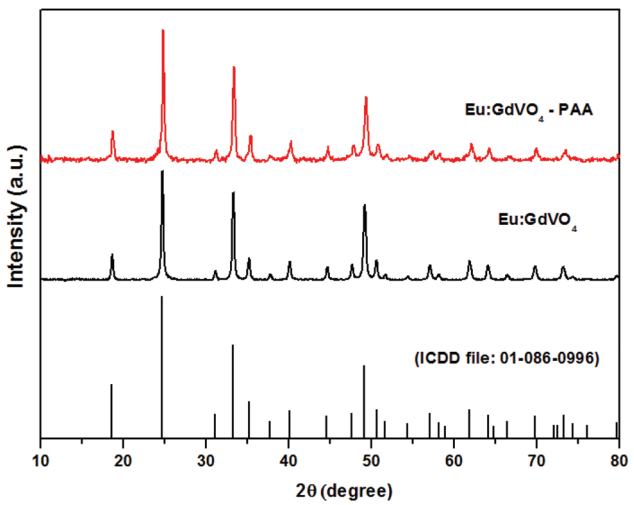

Fig. 2 X-ray diffraction patterns for the $Eu_{0.10}Gd_{0.90}VO_4$ nanocrystals unfunctionalized and functionalized with PAA. The reference pattern for tetragonal $GdVO_4$ obtained from the ICDD file is also included.

Table 1 Crystallite size, hydrodynamic diameter and zeta potential (measured at pH = 6.95) of Eu:$GdVO_4$ nanocrystals unfunctionalized and functionalized with AMD and PAA[a]

Samples	Hydrodynamic diameter/DLS (nm)	Zeta potential (mV)	Crystallite size (nm)
Eu:$GdVO_4$	70 (20)	−27.4	54
Eu:$GdVO_4$-AMD	134 (55)	+39.5	—
Eu:$GdVO_4$-PAA	60 (25)	−44.8	62

[a] The standard deviations are shown in parentheses.

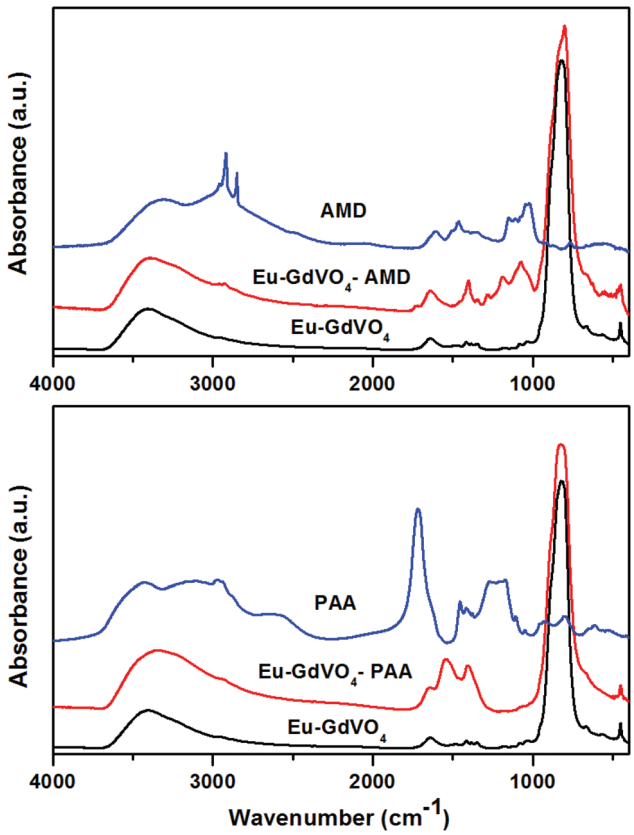

Fig. 3 Infrared spectra obtained for the $Eu_{0.10}Gd_{0.90}VO_4$ nanocrystals unfunctionalized and functionalized with AMD (top) and PAA (bottom). The spectra of amino-dextran and polyacrylic acid polymers are also included for comparison.

other Ln-doped nanoparticles prepared in EG,[13a] can be discarded in our case.

The photoluminescence properties of the Eu:$GdVO_4$ nanocrystals with different Eu content were evaluated in order to find the optimum nanophosphor. Fig. 5 (top) shows the excitation spectrum recorded for the $Eu_{0.10}Gd_{0.90}VO_4$ (10% Eu content) nanophosphors monitored at the most intense Eu^{3+} emission band (618 nm). As observed, it consisted of a strong broad band centered at 274 nm, which has been previously observed for several Eu-doped $LnVO_4$ systems[20–23] and attributed to the overlapping of two charge transfer (CT) processes involving Eu–O and V–O components, the former appearing at higher energy[21,24] or to electric and dipole-allowed transitions from the $^1A_2$ to the ^1E and $^1A_1$ excited states of the VO_4^{3-} ion.[20]

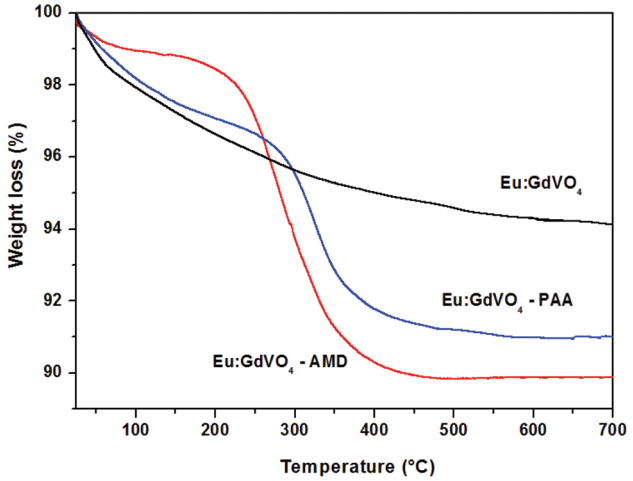

Fig. 4 TGA curve analyses for the $Eu_{0.10}Gd_{0.90}VO_4$ nanocrystals unfunctionalized and functionalized with AMD and PAA.

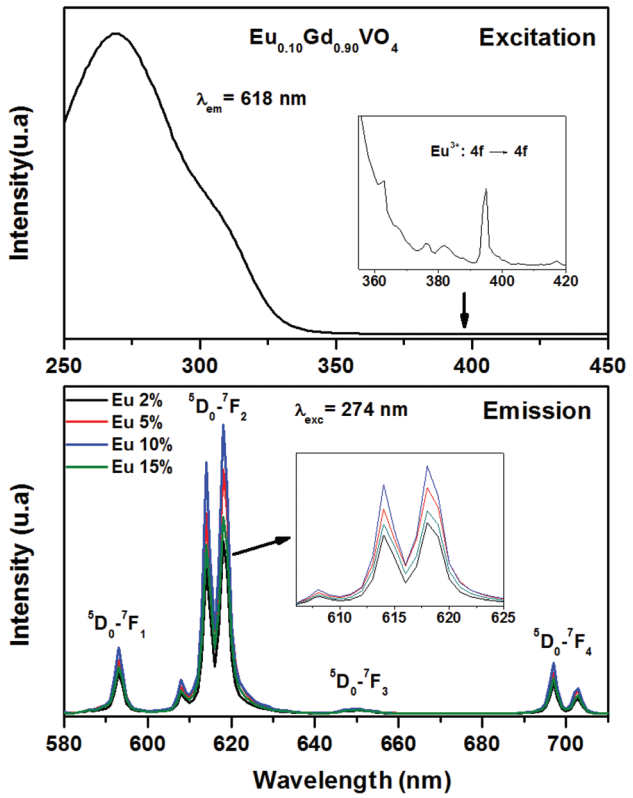

Fig. 5 Excitation (λ_{em} = 618 nm) spectrum for $Eu_{0.10}Gd_{0.90}VO_4$ nanocrystals (top) and emission (λ_{ex} = 274 nm) spectra of the Eu-doped $GdVO_4$ with different Eu content (bottom).

Some other bands resulting from f–f transitions of Eu^{3+} were also found (inset in Fig. 5, top), which were much weaker than those due to the CT processes, indicating that the excitation of Eu^{3+} is more efficient through the energy transfer band. Upon excitation at this band (λ_{ex} = 274 nm), the characteristic transition lines from the excited $^5D_0$ level of Eu^{3+} were detected (Fig. 5, bottom). As expected for this material,[24] the two most intense bands are those originating from $^5D_0$–$^7F_1$ (593 nm) and $^5D_0$–$^7F_2$ (618 nm) transitions, respectively, which were located in the 580–620 nm region. It should be noted that the most intense emission ($^5D_0$–$^7F_2$ transitions), which appeared split into two bands at 614 and 618 nm due to the crystal field,[20,21] showed a relative intensity much higher than that of the $^5D_0$–$^7F_1$ transitions, indicating that the Eu^{3+} cations are located in crystallographic sites with no inversion center as those with D_{2d} symmetry occupied by Gd^{3+} cations in tetragonal $GdVO_4$.[24] In Fig. 5 (bottom), it can be also observed that the increase of the Eu doping level from 2 to 10% gave rise to an important increase of the intensity of the emission bands as a consequence of the increase of the number of emission centers. However, such intensity decreased significantly when the Eu content was increased to 15% indicating the presence of a concentration quenching effect. Thus, the Eu doping level driving the strongest emission for our nanocrystals was 10% (Eu/Eu + Gd) mol ratio, which is within the range previously reported for Eu:$GdVO_4$ nanorods[24] and other more heterogeneous nanostructures.[20] Therefore, this sample was selected for further studies.

3.2. Functionalization of Eu:$GdVO_4$ nanocrystals

The $Eu_{0.10}Gd_{0.90}VO_4$ nanocrystals were functionalized with amino and carboxylate groups according to the two step and one-pot procedures described in the Experimental section.

The incorporation of AMD polysaccharide into the $Eu_{0.10}Gd_{0.90}VO_4$ nanocrystals following the two step method (functionalization was performed on previously synthesized nanocrystals) was substantiated by FTIR spectroscopy. Thus, the spectrum of the AMD functionalized nanocrystals (Fig. 3, top) displayed the absorption characteristics of the non-functionalized Eu:$GdVO_4$ nanocrystals above described, along with some other bands in the 1000–1500 cm^{-1} region and two weaker features at around 2930 cm^{-1}, which were also detected for the amino-dextran polymer (Fig. 3, top) and are mainly due to the O–C–O vibrations (1000–1200 cm^{-1}) and the CH_2 stretching vibrations of dextran, respectively,[25] indicating the effective absorption of AMD molecules on the surface of the nanoparticles.

Thermogravimetric analyses were used to estimate the amount of amino-dextran species attached to the nanoparticles surface. The TGA curve obtained for the Eu–$GdVO_4$ nanocrystals after AMD adsorption is reported in Fig. 4. It is seen that a mass loss occurred in a wide temperature range from room temperature to 700 °C which could be divided into two steps. The first one (~2 wt%) due to the water release took place from room temperature to about 230 °C. It should be noted that the amount of adsorbed water was lower in this case than for the non-functionalized nanoparticles. A second weight loss of ~8 wt% took place from 230 °C to 700 °C which is associated with the decomposition of the adsorbed organic species, mainly AMD polymers and carbonate anions coming from CO_2 adsorption. Since the weight content corresponding to the latter is ~2% (as determined above for non-

functionalized samples), it can be considered that the amount of AMD species on the surface of the nanoparticles corresponded to ~6 wt%.

The success of the functionalization was also confirmed by the surface charge reversal observed for the AMD functionalized nanoparticles in aqueous suspensions (*Z* potential = 39.5 mV) when compared with the untreated ones (*Z* potential = −27.4 mV) (Table 1).

The functionalization of the $Eu_{0.10}Gd_{0.90}VO_4$ nanocrystals with PAA polymers was carried out through a one-pot procedure involving the addition of PAA (2 mg cm^{-3}) to the starting solutions prior to the aging process required for the nanoparticles synthesis. Such addition was found to have an important effect on morphological characteristics of the final nanocrystals. Thus, almost equiaxial nanocrystals were obtained (Fig. 1, bottom) which were more homogeneous than those formed in the absence of PAA (Fig. 1, top). These nanocrystals also consisted of tetragonal $GdVO_4$ (Fig. 2) and were monocrystalline as indicated by the crystallite size value estimated from their XRD pattern, which was similar (62 nm) to the mean hydrodynamic diameter (60 nm) (Table 1) obtained from DLS (Fig. S3†).

In addition to the vibrational features due to the non-functionalized nanocrystals, the FTIR spectrum obtained for the PAA functionalized nanocrystals (Fig. 3, bottom) displayed some extra signals that confirm the presence of PAA on the surface of the nanoparticles. Thus, the bands around 1400 and 1550 cm^{-1} can be ascribed to the symmetric and asymmetric stretching frequencies of the carboxylate ion, respectively, which must be mainly due to the PAA species since their intensity is much higher than that of the carbonate impurities appearing in the same region for the unfunctionalized sample. For the same reason, the possible presence of such carbonate ions in the PAA-functionalized particles cannot be analysed on the basis of these data. It should be noted that the carboxylate bands appeared to be shifted to lower frequencies for pure PAA, which suggests that the carboxylate functional groups of the polymer are protonated, whereas in the nanoparticles they are mainly ionized.[26]

The TGA curve obtained for the PAA functionalized nanoparticles is shown in Fig. 4. As observed, the total mass loss was similar (~9 wt%) to that observed after functionalization with AMD (10%) and also took place in two steps. The first one (25–230 °C), due to the water release, was higher (~4 wt%) than that associated with the AMD-functionalized nanoparticles (~2 wt%) but similar to that obtained for the unfunctionalized ones (~4 wt%). The second loss (~5 wt%) occurred in the same temperature range observed for the AMD-functionalized nanoparticles (250–700 °C) and was also attributed to the decomposition of mainly PAA, although the presence of a small amount of carbonate anions cannot be discarded. The success of the functionalization was also confirmed by the increase of the surface charge value observed for the PAA functionalized nanoparticles (*Z* potential = −44.8 mV) when compared with the unfunctionalized nanocrystals (*Z* potential = −27.4 mV) (Table 1).

The effects of functionalization on the photoluminescence (PL) properties of the $Eu_{0.10}Gd_{0.90}VO_4$ nanophosphors were also investigated. Fig. 6 displays the excitation (monitored at 618 nm) and emission (λ_{ex} = 274 nm) spectra of the functionalized samples along with the spectra corresponding to the unfunctionalized sample for comparison. As observed, the intensity of the CT band decreased for both functionalized samples when compared with the unfunctionalized nanoparticles (Fig. 6, top). A similar behavior was also detected for the emission bands (Fig. 6, bottom). These effects might be ascribed to the presence of organic species on the nanoparticles surface, which are known to affect the luminescence properties of Eu since they increase the probability of non-radiative transition (not efficient transfer) due to their high vibrational frequencies,[27] resulting in a partial quenching of luminescence.

To confirm this suggestion, lifetimes of $^5D_0$ Eu manifold have been measured under the excitation provided by the second harmonic of a pulsed Nd:YAG laser (λ_{exc} = 532 nm). This excitation efficiently populates the $^5D_1$ multiplet ($^7F_0 \rightarrow {}^5D_1$ transition) which then populates the $^5D_0$ state *via* non-radiative relaxation,[28] from where the different visible emissions originate. It has been verified that the emission spectra under this excitation are coincident with those obtained after 274 nm excitation as shown in Fig. 6. The normalized

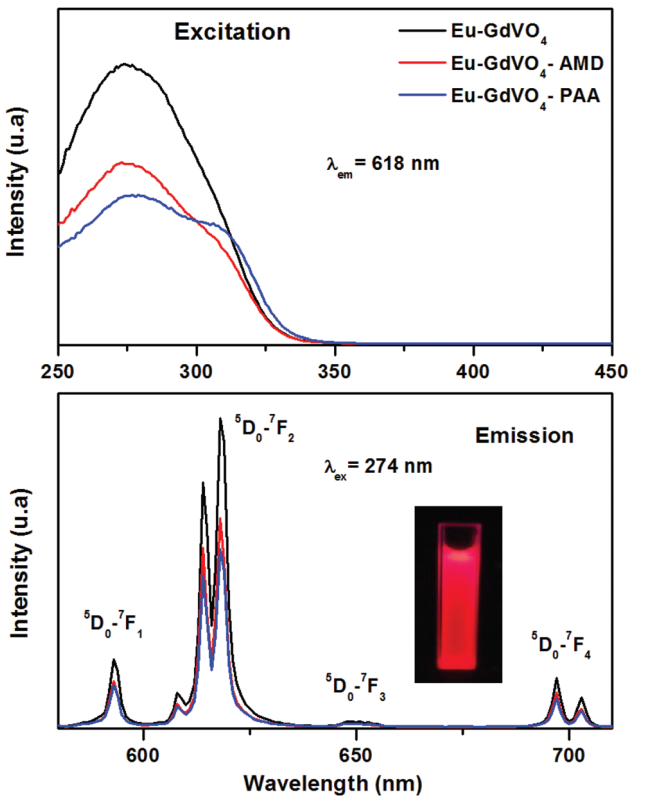

Fig. 6 Excitation spectra (λ_{em} = 618 nm) (top) and emission spectra (λ_{ex} = 274 nm) (bottom) recorded for unfunctionalized and functionalized $Eu_{0.10}Gd_{0.90}VO_4$ nanoparticles. Inset: photographs of an aqueous dispersion of $Eu_{0.10}Gd_{0.90}VO_4$ functionalized with PAA under UV (λ = 312 nm) illumination.

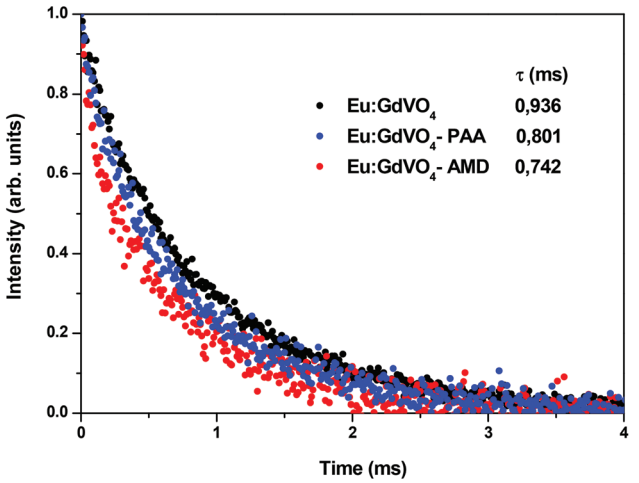

Fig. 7 Temporal evolution of the $^5D_0 \rightarrow {}^7F_2$ luminescence measured after pulsed excitation to the vanadate group in the Eu:$GdVO_4$ nanocrystals unfunctionalized and functionalized with AMD and PAA.

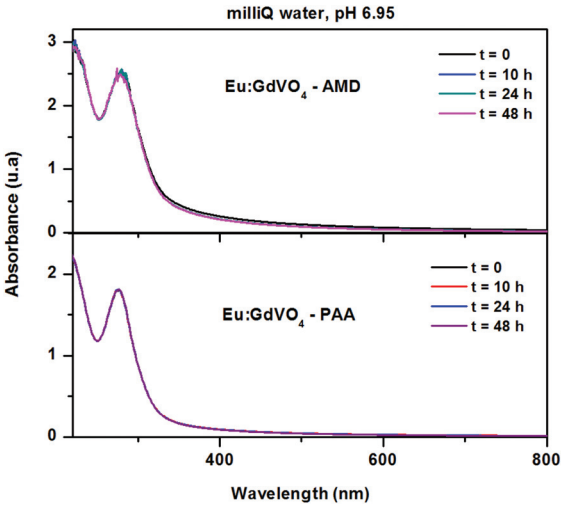

Fig. 8 Evolution with aging time of the UV-visible absorption spectra recorded for unfunctionalized and functionalized $Eu_{0.10}Gd_{0.90}VO_4$ nanocrystals dispersed in milliQ water (pH = 6.95).

temporal decays of the $^5D_0$ level, measured at λ_{em} = 618 nm ($^5D_0 \rightarrow {}^7F_2$ transition), for the unfunctionalized and the two functionalized samples are shown in Fig. 7. The emission lifetimes (τ) included in the inset of this figure have been evaluated from these measurements as:[29]

$$\tau = \int_0^\infty t\,I(t)\,\mathrm{d}t \Big/ \int_0^\infty I(t)\,\mathrm{d}t$$

As observed, the emission lifetime obtained for the functionalized samples was lower (0.8 ms, for the PAA functionalized sample and 0.74 ms, for the AMD functionalized sample) than that of the functionalized one (0.94 ms), confirming the partial luminescence quenching resulting from the functionalization process. It can be also observed that the lifetime decrease is slightly higher for the AMD-functionalized sample than for the PAA-functionalized sample, which retained a strong red luminescence when illuminated with UV radiation (312 nm), as is illustrated in the inset of Fig. 6. Therefore, these modified Eu-doped $GdVO_4$ nanocrystals may be used as optical biolabels for "*in vitro*" applications.

3.3. Colloidal stability

The functionalization with AMD by subsequent covering of the $Eu_{0.10}Gd_{0.90}VO_4$ nanoparticles previously obtained had a significant effect on the hydrodynamic diameter of the nanocrystals measured by DLS (Fig. S3†). Thus, the value of this magnitude obtained from freshly prepared dispersions in water (pH = 6.95) was clearly higher (134 nm) than that obtained from the unfunctionalized nanocrystals (70 nm) (Table 1), which cannot be only explained by the existence of AMD on the nanoparticles surface but most probably by the presence of a weak aggregation process since no changes in particle size were observed under the TEM microscope after functionalization (Fig. S4†). It should be noted that the value of hydrodynamic diameter remained almost constant (123 nm) after keeping the dispersion undisturbed for 2 weeks indicating that the above suggested aggregation should take place in the course of functionalization. In spite of the aggregation, no sedimentation was detected in the suspensions after at least 2 days, as indicated by the lack of variation of the intensity of the band due to vanadate ions appearing at ~270 nm in their UV-visible absorption spectrum (Fig. 8). A similar behavior was observed for water suspensions (pH = 6.95) of the $Eu_{0.10}Gd_{0.90}VO_4$ nanoparticles functionalized with PAA, whose UV-visible absorption spectrum also remained constant on aging up to at least 2 days (Fig. 8). It is important to mention that for the latter system, the hydrodynamic diameter measured for the suspension kept undisturbed for two weeks was quite similar (55 nm) to that obtained for fresh dispersions (60 nm) indicating the absence of particle aggregation during this period of time and the higher colloidal stability of the $Eu_{0.10}Gd_{0.90}VO_4$–PAA nanophosphors. The stability of the latter sample in one of the most used biological buffer media (MES at pH = 6.5) and in completed cell culture media (DMEM + FBS) was also addressed. It was found that in MES buffer, no sedimentation took place during at least 4 days of aging (Fig. 9, bottom) and that the average hydrodynamic diameter of the nanoparticles remained unaltered (60 nm) after the same period of time (Fig. 9, top), whereas in completed cell culture media (DMEM + FBS), a slight increase in this magnitude was detected (78 nm).

Owing to this excellent colloidal stability of the $Eu_{0.10}Gd_{0.90}VO_4$–PAA nanophosphors, they were selected for studies on their biocompatibility and suitability as MRI contrast agents.

3.4. Relaxation time studies

The measurement of the longitudinal (T_1) and transversal (T_2) proton relaxation times as a function of the gadolinium ion concentration at 1.5 T gave for the PAA functionalized $Eu_{0.10}Gd_{0.90}VO_4$ sample r_1 and r_2 values of 0.77 and 2.28 s^{-1} mM^{-1},

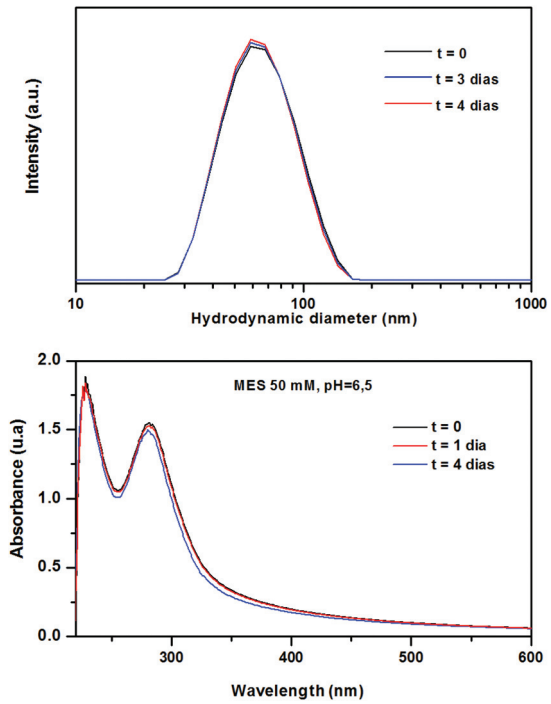

Fig. 9 Hydrodynamic diameter obtained by DLS measurements (top) and evolution with aging time of the UV-visible absorption spectra (bottom) for the PAA functionalized $Eu_{0.10}Gd_{0.90}VO_4$ nanocrystals in biological buffer media (MES at pH = 6.5).

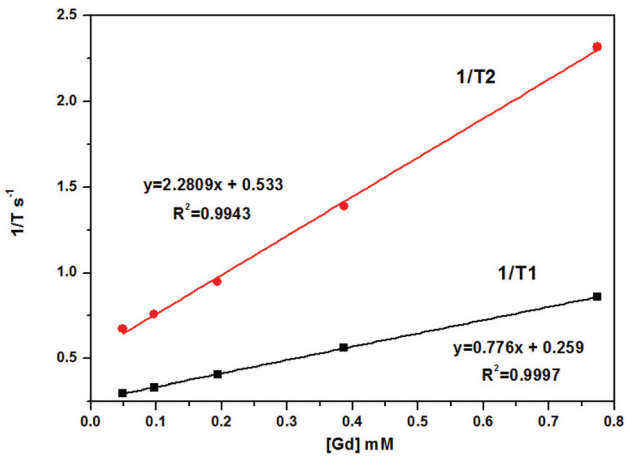

Fig. 10 Proton relaxivities (r_1 and r_2) measured for the $Eu_{0.10}Gd_{0.90}VO_4$ nanophosphor functionalized with PAA at 1.5 T.

respectively (Fig. 10). It must be first mentioned that these values are quite similar to those obtained for the unfunctionalized sample (Fig. S5†), which indicates that the functionalization process had no important effect on the magnetic behavior of this material. It must be also noted that the r_1 value measured for our nanoparticles is among the highest values previously reported for this system (between 0.438 and 0.76 s^{-1} mM^{-1}),[13b,14] although the applied field used for the measurements was different in all cases (0.5,[14] 1.5 (this work) and 4.7 T[13b]), which complicates a proper comparison of these

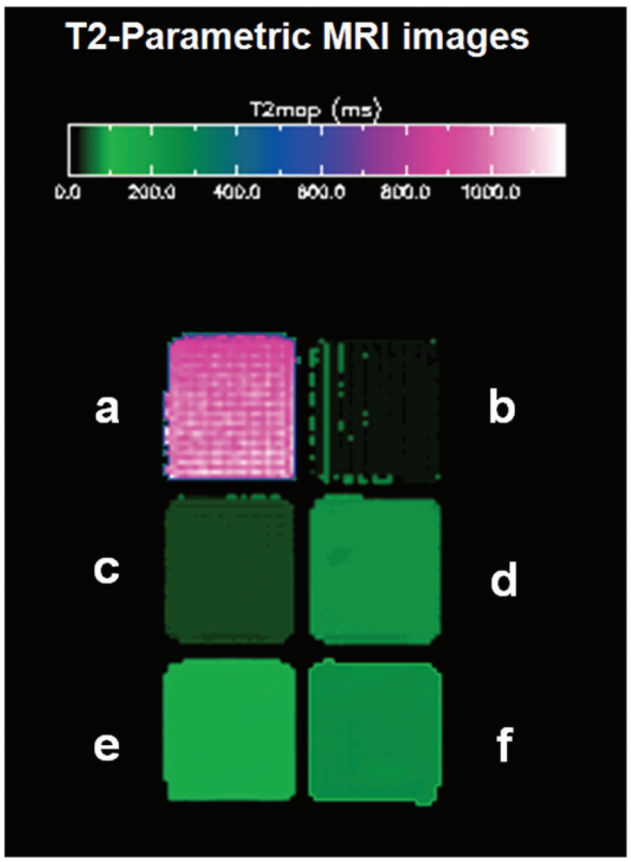

Fig. 11 T_2 parametric MRI phantom images (9.4 T) of $Eu_{0.10}Gd_{0.90}VO_4$ nanophosphor functionalized with PAA showing transversal relaxation times of nanoparticle suspensions: (a) control (water); (b–f) serial dilutions (0.1, 0.05, 0.025, 0.0125, 0.00625 mg cm^{-3}).

values since they are affected by these parameters among other factors.[30] Nevertheless, the r_2/r_1 ratio obtained for our nanoparticles was rather high (~3) precluding their use as positive contrast agents, which requires r_2/r_1 values close to unity.[1h,9a] However, the MRI phantom analysis (Fig. 11) clearly manifested T_2 susceptibility effects at higher magnetic fields (9.4 T) indicating that our Eu:$GdVO_4$ nanoparticles may be used as negative (T_2-weighted) MRI contrast agents.

3.5. Biocompatibility studies of Eu:$GdVO_4$ nanocrystals functionalized with PAA

Biocompatibility studies were performed by evaluating the cell viability of Vero cells by the MTT assay.[31] This assay relies on the mitochondrial activity of fibroblasts and represents a parameter for their metabolic activity. The MTT (3-(4,5-dimethylthiazol-2-yl)-2,5-diphenyltetrazolium bromide) assay is a simple non-radioactive colorimetric assay to measure cell cytotoxicity, proliferation, or viability. MTT is a yellow, water-soluble tetrazolium salt. Metabolically active cells are able to convert this dye into a water-insoluble dark-blue formazan by reductive cleavage of the tetrazolium ring. Formazan crystals, then, can be dissolved in an organic solvent such as dimethylsulphoxide (DMSO) and quantified by measuring the

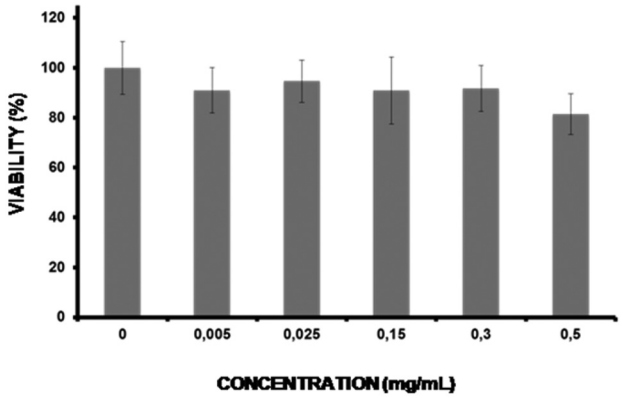

Fig. 12 Cytotoxicity profiles of the $Eu_{0.10}Gd_{0.90}VO_4$–PAA nanoparticles with VERO cells as determined by the MTT assay. Percentage of viability of cells was expressed relative to control cells (n = 5). Results are represented as mean ± standard deviations.

absorbance of the solution at 550 nm, and the resultant value is related to the number of living cells. The metabolic activity and proliferation of fibroblasts were thus measured after 24 hours culture, and showed negligible toxicity effects (Fig. 12) with viability percentages >80% for concentrations up to 0.5 mg cm^{-3}. Similar results were obtained when the fibroblasts proliferation was measured after longer incubation times (120 hours), which are closer to the final application of this kind of nanoparticles. These MTT assay results show the possibility of using this kind of nanoparticles for long term fluorescent or MRI analysis and tracking into cells or tissues. However, a deeper viability and toxicological study should be performed to guarantee the lack of adverse effects on the organism.

4. Conclusions

Eu-doped $GdVO_4$ nanocrystals (~70 nm) with almost equiaxial morphology have been synthesized by a homogenous precipitation process using ethylene glycol–water as a solvent at relatively low temperature. These nanoparticles consisted of single crystals with tetragonal structure. Luminescence measurement reveals that the optimum Eu doping level was 10% (Eu/Eu + Gd) molar ratio. These nanocrystals were successfully functionalized with amino (two steps) and carboxylate (one-pot) groups provided by amino-dextran polymers (AMD) and polyacrylic acid (PAA), respectively, which allows further conjugation with biologically active molecules (such as antibodies, peptides and proteins). After functionalization, the $Eu_{0.10}Gd_{0.90}VO_4$ samples retained a strong luminescence under UV illumination (312 nm). It was also found that the functionalization with AMD gave rise to a certain degree of aggregation, which was not observed for the PAA-functionalized sample. The latter also showed a very high colloidal stability in neutral water, biological buffer (MES, pH = 6.5) and in cell culture media dispersions as well as no significant toxicity for cells in concentrations up to 0.5 mg cm^{-3}. These properties make the PAA-functionalized Eu–$GdVO_4$ nanocrystals good candidates as optical biolabels for "*in vitro*" applications. Finally, magnetic relaxivity measurements and phantom analyses revealed that they may be used as negative (T_2-weighted) MRI contrast agents.

Acknowledgements

This work has been supported by Junta de Andalucía (grant FQM6090), the Spanish CICYT (grant MAT2011-23593), Fondo Social Europeo and ERC-Starting Grant NANOPUZZLE. Nuria O. Nuñez wants to thank the Spanish National Research Council for financial support (PIE-200960I127). The authors also want to thank Prof. Fernando Cussó for his help for lifetime measurements.

References

1 (*a*) G. Tian, Z. Gu, X. Liu, L. Zhou, W. Yin, L. Yan, S. Jin, W. Ren, G. Xing, S. Li and Y. Zhao, *J. Phys. Chem. C*, 2011, **115**, 23790; (*b*) J. W. Mulder, A. W. Griffioen, G. J. Strijkers, D. P. Cormode, K. Nicolay and Z. A. Fayad, *Nanomedicine*, 2007, **2**, 307; (*c*) R. Kumar, M. Nyk, T. Y. Ohulchanskyy, C. A. Flask and P. N. Prasad, *Adv. Funct. Mater.*, 2009, **19**, 853; (*d*) G. K. Das, B. C. Heng, S. C. Ng, T. White, J. S. Loo, L. D'Silva, P. Padmanabhan, K. K. Bhakoo, S. T. Selvan and T. Y. Tan, *Langmuir*, 2010, **26**, 8959; (*e*) J. Ryu, H. Y. Park, K. Kim, H. Kim, J. H. Yoo, M. Kang, K. Im, R. Grailhe and R. Song, *J. Phys. Chem. C*, 2010, **114**, 21077; (*f*) Y. I. Park, J. H. Kim, K. T. Lee, K. S. Jeon, H. B. Na, J. H. Yu, H. M. Kim, N. Lee, S. H. Choi, S. I. Baik, H. Kim, S. P. Park, B. J. Park, Y. W. Kim, S. H. Lee, S. Y. Yoon, I. C. Song, W. K. Moon, Y. D. Suh and T. Hyeon, *Adv. Mater.*, 2009, **21**, 4467; (*g*) X. Yu, Y. Shan, G. Li and K. Chen, *J. Mater. Chem.*, 2011, **21**, 8104; (*h*) N. J. J. Johnson, W. Oakden, G. J. Stanisz, R. S. Prosser and F. C. J. M. van Veggel, *Chem. Mater.*, 2011, **23**, 3714; (*i*) M. He, P. Huang, C. Zhang, H. Hu, C. Bao, G. Gao, R. He and D. Cui, *Adv. Funct. Mater.*, 2011, **21**, 4470; (*j*) L. Zhou, Z. Gu, X. Liu, W. Yin, G. Tian, L. Yan, S. Jin, W. Ren, G. Xing, W. Li, X. Chang, Z. Hu and Y. Zhao, *J. Mater. Chem.*, 2012, **22**, 966.
2 F. Wang, X. Chen, Z. Zhao, S. Tang, X. Huang, C. Lin, C. Cai and N. Zheng, *J. Mater. Chem.*, 2011, **21**, 11244.
3 Z. Liu, G. Yi, H. Zhang, J. Ding, Y. Zhang and J. Xue, *Chem. Commun.*, 2008, 694.
4 Z. Y. Ma, D. Dosev, M. Nichkova, S. J. Gee, B. D. Hammock and I. M. Kennedy, *J. Mater. Chem.*, 2009, **19**, 4695.
5 Y. Zhang, G. K. Das, R. Xu and T. T. Tan, *J. Mater. Chem.*, 2009, **19**, 3696.
6 J. L. Bridot, A. C. Faure, S. Laurent, C. Rivière, C. Billotey, B. Hiba, M. Janier, V. Josser, J. J. Coll, L. V. Elst, R. Muller, S. Roux, P. Perriat and O. Tillement, *J. Am. Chem. Soc.*, 2007, **129**, 5076.

7 F. Evanics, P. R. Diamente, F. C. J. M. van Veggel, G. J. Stanisz and R. S. Prosser, *Chem. Mater.*, 2006, **18**, 2499.
8 K. M. L. Taylor, J. S. Kim, W. J. Rieter, H. An and W. Lin, *J. Am. Chem. Soc.*, 2008, **130**, 2154.
9 (*a*) H. Hifumi, S. Yamaoka, A. Tanimoto, D. Citterio and K. Suzuki, *J. Am. Chem. Soc.*, 2006, **128**, 15090; (*b*) M. F. Dumont, C. Baligand, Y. Li, E. Knowles, M. W. Meisel, G. A. Walter and D. R. Talham, *Bioconjugate Chem.*, 2012, **23**, 951; (*c*) W. Ren, G. Tian, L. Zhou, W. Yin, L. Yan, S. Jin, Y. Zu, S. Li, Z. Gu and Y. Zhao, *Nanoscale*, 2012, **4**, 3754.
10 (*a*) D. Giaume, M. Poggi, D. Casanova, G. Mialon, K. Lahlil, A. Alexandrou, T. Gacoin and J. P. Boilot, *Langmuir*, 2008, **24**, 11018; (*b*) L. Yang, G. Li, W. Hu, M. Zhao, L. Sun, J. Zheng, T. Yan and L. Li, *Eur. J. Inorg. Chem.*, 2011, 2211; (*c*) B. K. Gupta, V. Rathee, T. N. Narayan, P. Thanikaivelan, A. Saha, S. P. Singh, V. Shanker, A. A. Narti and P. M. Alayan, *Small*, 2011, **7**, 1767.
11 (*a*) M. Gu, Q. Liu, S. Mao and C. Chang, *Cryst. Growth Des.*, 2008, **8**, 1422; (*b*) Y. Zheng, H. You, G. Jia, K. Liu, Y. Song, M. Yang and H. Zhang, *Cryst. Growth Des.*, 2009, **9**, 5101; (*c*) Y. Su, L. Liping, G. Li, J. Liu, X. Chen, W. Hu and G. Liu, *J. Nanosci. Nanotechnol.*, 2010, **10**, 1877.
12 R. Calderon-Villajos, C. Zaldo and C. Cascales, *CrystEngComm*, 2012, **14**, 2756.
13 (*a*) N. Shanta Singh, R. S. Ningthoujam, G. Phaomei, S. Dorendrajit, A. Vinu and R. K. Vatsa, *Dalton Trans.*, 2012, **41**, 4412; (*b*) W. Yin, L. Zhou, Z. Gu, G. Tian, S. Jin, L. Yan, X. Liu, G. Xing, W. Ren, F. Liu, Z. Pan and Y. Zhao, *J. Mater. Chem.*, 2012, **22**, 6974.
14 X. Kang, D. Yang, Y. Dai, M. Shang, Z. Cheng, X. Zhang, H. Lian, P. Ma and J. Lin, *Nanoscale*, 2013, **5**, 253.
15 X. Kang, D. Yang, P. Ma, Y. Dai, M. Shang, D. Geng, Z. Cheng and J. Lin, *Langmuir*, 2013, **29**, 1286.
16 D. K. Chatterjee, M. K. Gnanasammandhan and Y. Zhang, *Small*, 2010, **6**, 2781.
17 B. J. Shen, L. D. Sun, J. D. Zhu, L. H. Wei, H. F. Sun and C. H. Yan, *Adv. Funct. Mater.*, 2010, **20**, 3708.
18 R. C. Rodríguez, J. M. Bolivar, G. Volpato, M. Filice, C. Godoy, R. Fernandez-Lafuente and J. M. Guisan, *J. Biotechnol.*, 2009, **144**, 113.
19 L. Yang, L. Li, M. Zhao and G. Li, *Phys. Chem. Chem. Phys.*, 2012, **14**, 9956.
20 S. Tang, M. Huang, J. Wang, F. Yu, G. Shang and J. Wu, *J. Alloys Compd.*, 2012, **513**, 474.
21 K. Riwotzki and M. Haase, *J. Phys. Chem. B*, 1998, **102**, 10129.
22 N. Shanta Singh, R. S. Ningthoujam, D. L. Romila, N. Yaiphaba, V. Sudarsan, S. Dorendrajit Singh, R. K. Vatsa and R. Tewari, *J. Appl. Phys.*, 2008, **104**, 104307.
23 M. Kim and S. Kang, *J. Mater. Res.*, 2007, **22**, 1.
24 L. Yang, G. Li, M. Zhao, J. Zheng, X. Guan and L. Li, *Nanotechnology*, 2012, **23**, 245602.
25 W. Chen, P. Yi, Y. Zhang, L. Zhang, Z. Deng and Z. Zhang, *ACS Appl. Mater. Interfaces*, 2011, **3**, 4085.
26 L. J. Kirwan, P. F. Fawell and W. Bronswijk, *Langmuir*, 2003, **19**, 5802.
27 P. Yang, S. Huang, D. Kong, J. Lin and H. Fu, *Inorg. Chem.*, 2007, **46**, 3203.
28 S. Rodríguez-Liviano, F. J. Aparicio, T. C. Rojas, A. B. Hungría, L. E. Chinchilla and M. Ocaña, *Cryst. Growth Des.*, 2012, **12**, 635.
29 M. Inokuti and F. J. Hirayama, *Chem. Phys.*, 1965, **43**, 1978.
30 P. Caravan, C. T. Farrar, L. Frullano and R. Uppal, *Contrast Media Mol. Imaging*, 2009, **4**, 89.
31 T. J. Mosmann, *J. Immunol. Methods*, 1993, **95**, 55.

